

STUDY OF PRECESSING VORTEX CORE DURING VORTEX BREAKDOWN USING LES AND POD

Christophe Duwig

Div. of Fluid Mechanics, Dept. Energy Sciences
Lund University – Box 118
SE- 22100 Lund, Sweden
Christophe.Duwig@vok.lth.se

Laszlo Fuchs

Div. of Fluid Mechanics, Dept. Energy Sciences
Lund University – Box 118
SE- 22100 Lund, Sweden
Laszlo.Fuchs@vok.lth.se

ABSTRACT

Modeling and understanding the vortex breakdown is a key issue of modern Lean Premixed Combustors. The main difficulty of the problem is the unsteady behavior of this type of flow: Large structures resulting from vortex breakdown and the swirling shear-layers, affect directly the flame stabilization leading to heat-release fluctuations and combustion instabilities. Consequently, one needs to capture and understand turbulent coherent structures dynamics for designing efficient burners. This task is particularly challenging since it deals with capturing coherent motions within a chaotic system. This requires the use of state-of-the-art numerical and experimental techniques.

The present work focuses on the numerical study of isothermal vortex breakdown using Large Eddy Simulation (LES) for obtaining a 4D description of the flow. A sensitivity analysis and further comparisons with experimental data indicate that the LES tool captures accurately the flow. The LES results are then processed for capturing and identifying the coherent structures. The characteristic frequencies are analyzed. Also with this respect good agreement with data from the literature is obtained. The large scale vortices have been visualized providing a good insight into the unsteady flow pattern. Finally, Proper Orthogonal Decomposition (POD) has been applied to the 4D LES data in order to identify the contribution of different modes. The presence of the Precessing Vortex Core (PVC) corresponding to a pair of helical structures is identified and is highlighted.

INTRODUCTION

Swirling flow plays a central role in many industrial applications. For example, modern combustors are based on an aerodynamic type of flame holding and thereby eliminating the need for any additional bluff body. Instead, a swirling motion is given to the fresh gas jet. A swirling jet is subject to centrifugal forces leading to a radial expansion of the jet. Due to the entrainment of gas into the jet a low-pressure region appears around the axis region, close to the expansion. If the swirling motion is strong enough, the longitudinal pressure gradient induces an axial back flow

bringing burnt hot gases towards the fresh gases, and thereby stabilizing the flame. As the flow reverses the axial vortex (of the swirling jet) disappears from the axis which effect is termed as vortex break-down. Unfortunately, the resulting flow field is inherently unsteady. Consequently, modeling and understanding of the vortex breakdown is then a key issue in flame stabilization.

Despite of more than 40 years of research, the details of the mechanism related to vortex break down are only partially understood (Lucca-Negro and O'Doherty, 2001). The main difficulty of the problem is the unsteady behavior of this type of flow: Large structures resulting from vortex breakdown and the swirling shear-layers, affect directly the central recirculation zone. These structures cause large deterministic fluctuations in the flow field. Examples of large unsteady motions occurring during vortex breakdown can be found in the literature, e.g. (Dellenback et al., 1988; Syred, 2006; Cala et al., 2006; Fernandes et al., 2006). A large scale unsteady motions arising during vortex breakdown of interest in this paper is the Precessing Vortex Core (PVC). Experimental and numerical works (see a recent review (Syred, 2006)) have reported that vortex breakdown might result in an off-axis precession of the central recirculation zone. The recirculation zone undergoes a periodic rotational and translational (i.e. spiral) motion around the axis and the instantaneous flow field is far from being axi-symmetric. However, time averaging the flow also maintains the geometrical axi-symmetry. Several works (Syred, 2006) highlighted the need to capture and understand turbulent coherent structures dynamics. This task is particularly challenging since it deals with capturing coherent motions within a chaotic system and should be done using state-of-the-art numerical and experimental techniques.

The present work focuses on the study of isothermal vortex breakdown occurring through an abrupt expansion. The numerical case corresponds to a geometry studied by Dellenback et al. (1988) using Laser Doppler Velocimetry (LDV). Firstly, the numerical tool, closures and post-processing procedures are presented. A sensitivity analysis with respect to numerical and inflow conditions, is performed. The flow is characterized using mean of velocity

vector field and the root-mean-squared (RMS) of the fluctuations. The results are compared to available LDV data. The final section of the paper is devoted to the analysis of the unsteady flow features. Power spectra, phase diagram as well as proper orthogonal decomposition (POD) are used to extract information from the LES results so as to better understand the dynamics of the coherent structures.

NUMERICAL TOOL

LES equations and closure

In the LES framework, we consider the incompressible continuity and Navier-Stokes equations describing an isothermal low-mach number flow are (Sagaut, 2001):

$$\nabla \cdot \bar{u} = 0 \quad (1)$$

$$\frac{\partial \bar{u}}{\partial t} + \nabla \cdot (\overline{uu}) = -\frac{1}{\rho_0} \nabla p + \nabla \cdot (\overline{uu} - \overline{uu} + \nu \nabla \bar{u}) \quad (2)$$

where u is the velocity vector, ρ_0 the density (constant), p the pressure and ν the kinematic viscosity. The overbar denotes the “low-pass” LES spatial filter. It removes all the Fourier components that have shorter length scale than the filter size. The filtering operator is linear and is assumed to be commutative with the time- and space-derivatives. The filtering operation is not commutative with non-linear terms. Thus, filtering the non-linear terms leads to expressions that cannot be expressed in terms of the filtered quantities. These terms are gathered on the right-hand side in the equations above and that expression is denoted as the subgrid scale (SGS) term.

The main role of the SGS terms is to account for the interaction between the resolved and the unresolved scales. In the momentum equations, the SGS terms should account for the dissipative character of the small (unresolved) scales as well as for the transfer of energy among the resolved and unresolved scales. A computational grid can support only Fourier components that have longer wavelengths than the grid size. Thus, a dependent variable that is represented on a grid together with a discrete approximation for the derivatives in the governing equations leads to an *implicit* filtering. If no explicit SGS terms are added, then the numerical scheme should account at least for the small scale dissipation. This is attained for any numerically stable scheme. This type of approach has different names in the literature, e.g. *Implicit LES* (ILES) in Fureby and Grinstein, (2002). Too dissipative numerical schemes are highly inappropriate for LES since in addition to dissipation on small scales, they may be also dissipative on the resolved, larger scales. This effect can be avoided by choosing appropriate (higher order) discretization schemes. Here, we use a higher-order discretization scheme (Gullbrand et al., 2001). In addition, the spatial resolution has to be fine enough, virtually of the order of magnitude of the Taylor micro-scale. With such a resolution, the energy transfer among the large- and small-scales is dissipation independent at least in the mean, by Kolmogorov’s theory. Thus, the numerical scheme may act implicitly as a SGS model (Fureby and Grinstein, 2002) at least with respect to small scale scheme independent dissipation.

LES code

We use a high-order finite difference code that solves the incompressible Navier-Stokes equations on Cartesian grids (Gullbrand et al., 2001). The spatial discretization is done using a fourth order centered scheme except for the convective terms in equations (2) that are treated using a third-order upwind scheme. A second order implicit finite difference scheme is used for time discretization. Locally refined grids are employed in regions with large gradients. Multi-grid iterations are used to solve the implicit parts of the system. More details can be found in Gullbrand et al. (2001). Using Cartesian finite differences techniques provides fast and accurate results. These advantages make the present approach suitable for LES of turbulent flows.

Post processing tools

A commonly followed post-processing procedure consists of computing mean and RMS fields of the velocity variables. However, information related to large scale coherent motions is lost. We seek to supplement the mean and RMS fields by extracting statistical quantities out of Gigabytes of data generated by the LES. Following pioneer work of Lumley (Berkooz et al., 1991), we use the Proper Orthogonal Decomposition (POD). We focus on the most kinetic energy containing eddies/ modes. Consequently, one seeks to project the turbulent flow field on a vector base that maximizes the turbulent kinetic energy content for any subset of the base. It allows an accurate description of the turbulent data using only few modes (Berkooz et al., 1991). Given a vector Q containing the field variables and a vector base Φ , the POD gives:

$$Q(x, t) = Q^N(x, t) = \sum_{i=0}^N a_i(t) \Phi_i(x) \quad (3)$$

Note that the approximation Q^N of the turbulent data set Q converges to Q when N goes to infinity and that mode $i=0$ corresponds to the time averaged field.

The base vectors are computed so that they satisfy the eigenvalue problem (Berkooz et al., 1991):

$$\langle Q(x, t) \otimes Q^T(x, t) \rangle \Phi_i(x) = \lambda_i \Phi_i(x) \quad (4)$$

where the superscript T denotes the transposed of the vector and $\langle \cdot \rangle$ is the time averaging operator. It is worth noticing that the vectors Φ are the eigenvectors of the temporal auto-correlation tensor. The eigenvalue λ_i characterizes the turbulent kinetic energy content of the mode i . For practical reasons, it is seldom possible to solve Equation (4) if the turbulent data set is large. Instead, one may reduce the computational costs by using Sirovich’s *method of snapshots* e.g. (Smith et al., 2005).

The vortex core is visualized using criteria based on the second eigenvalue of the second invariant of the velocity derivatives tensor proposed by Jeong and Hussain (1995) (the so-called λ_2 technique). The vortex core is enclosed by a region where the second eigenvalue (λ_2) is negative.

COMPUTATIONAL CASE

Geometry and computational grid

We consider a model combustor corresponding to the experiments conducted by Dellenback et al. (1988). The

setup consists of a swirling jet of diameter D issuing into co-axial cylinder of diameter $2D$. It can also be describe as an axi-symmetric step of height $0.5D$. We restrict our study to a single case reported by Dellenback et al. (1988) with a Reynolds number based on the bulk velocity $Re=U_0D/\nu=3\cdot 10^5$ and a jet swirl number (based on the momentum fluxes) of $S=0.6$.

The computational domain is a $12D*2D*2D$ box starting at the $2D$ upstream of the expansion where measured velocity profiles. The computational grids contain $\sim 1\cdot 10^6$ (Grid A) and $\sim 2\cdot 10^6$ (Grid B) mesh-points with 50 and 66 cells across the diameter D , respectively. We estimate the Taylor turbulence micro-scale to be around $\sim D/50$ indicating that the implicit grid filter length lies well in the inertial subrange of the turbulent spectrum. In addition, we note that the present resolution is well in line with previous simulations reported in the literature e.g. (Schlüter et al., 2004).

In order to maintain time accuracy, the time step is set so that the Courant number is at most 0.3. All data are normalized by the bulk velocity U_0 and the pipe diameter D . The corresponding time unit τ is $\tau=D/U_0$ and the non-dimensional frequency or Strouhal number is $St=f\tau$. The time averaged quantities are computed over a time span of 25 000 time iterations or $\sim 200\tau$. For the POD, we use ~ 600 snapshots collected over $\sim 250\tau$. We note that increasing the number of snapshots above ~ 400 does not change significantly the first four modes.

Boundary conditions

The particular choice of boundary conditions is crucial for all computational results and in particular for LES. Swirling flows might be highly sensitive even to small variations in the temporal or the spatial form of the inlet conditions. One may also approximate the flow using a well defined (mean) velocity profile (from LDV for example) and adding artificially generated turbulent fluctuations. In fact, due to the uncertainty in experimental conditions, it is not very constructive to strive for the exact reconstruction of the experimental conditions. Instead, it is more important to assess the sensitivity of the results to the uncertainty in the boundary conditions. We consider the decomposition:

$$\bar{u}(x,t) = \langle u_{LDV} \rangle(x) + u'(x) \cdot F(t) \quad (5)$$

If $u'(x)$ is set to 0, we retrieve the quasi-laminar (QL) technique tested by Schlüter et al. (2004). Another alternative is to set $u'(x)$ in order to recover the fluctuation levels measured by LDV. This requires that the function $F(t)$ provides a seemingly turbulent fluctuation (STF). Here, we use a digital filter based technique (Klein et al., 2003). Equation (5) is set as inflow boundary on a plane located $2D$ upstream from the expansion ($x/D=-2$). Both alternatives (QL vs. STF) have been used in order to assess the sensitivity of the results to the inflow boundary conditions.

At the outlet, the flow is assumed to have a mass conservative zero gradient. Since the code uses a staggered grid, no explicit boundary condition is needed for the pressure field.

The different computational cases are summarized in Table 1.

Table 1: Summary of the computational cases.

Case	Re	Grid	Inflow
1	300000	A	QL
2	300000	B	QL
3	300000	A	STF

RESULTS AND DISCUSSION

Figure 1 shows the normalized axial velocity field in the model combustor both at a randomly chosen time step and on average. The instantaneous flow field is irregular, asymmetric and exhibits steep gradients as expected for a turbulent flow. In contrast, the mean flow field is smooth and axi-symmetric. The mean field has also two recirculation zones downstream of the expansion: a central recirculation zone (CRZ) that develops around the axis and a second, of toroidal shape, recirculation zone (TRZ) located just down-stream of the step.

Sensitivity analysis and comparison with LDV data

Figure 2 shows the normalized axial velocity from cases 1 to 3 plotted along radial lines. The 3 data sets agree well together showing the same trends and levels for both the mean and RMS fields. Case 3 exhibits somehow higher fluctuation levels as expected with the STF inflow conditions. Note that having the inflow $2D$ upstream of the expansion allows turbulence to develop upstream for the monitoring lines. Beside the strong shear associated with this type of flow is sufficient for producing strong fluctuations within $\sim 2D$. Therefore, the influence of the inflow fluctuations is not found to be significant in the present case. In addition, the present results also assess that the grid resolution does not affect significantly the results indicating the present computational grids are suitable for performing LES.

Figure 2 also presents the axial velocity together with the LDV measurements of Dellenback et al. (1988). The agreement is reasonably good showing that the LES captures well the two recirculation zones both in term of size and strength. The LES results seem to over-estimate the velocity of the annular swirling jet close to the expansion. The annular jet opening angle as well as the shear-layer locations is well captured. A similar feature is seen on Figure 3 presenting the azimuthal velocity component. The swirling velocity is over-estimated close to expansion. As a consequence, the shear-layers are stronger and the velocity fluctuations are higher. This effect is seen on both Figure 2 and 3 looking at the RMS of the velocity fluctuations. It explains the over-estimation of the fluctuation levels by the LES. However, the LES results capture the trend of the fluctuation fields. In particular the peak of azimuthal velocity fluctuation along the axis is well captured. As pointed out by Cala et al. (2006), the strong fluctuation of azimuthal velocity corresponds to the precessing vortex core (PVC) indicating that the simulations capture the PVC.

Analysis of the unsteady flow features

As shown above, large scale coherent structures like the PVC are responsible for large amplitudes fluctuations ($\sim 0.5U_0$) that are of the order of the mean velocity field. The

time averaging procedure hides important and dominant features of the flow and one seeks alternative statistical quantities enabling to characterize the coherent structures. The effects of these structures are seen on Figure 4 plotting the time evolution of the normalized axial velocity along a radial line. One clearly sees an intermittent behavior at $r/D \sim 0.5$ with dark and white pockets passing the sampling location. One may estimate the time between two pockets to be $\sim 1.6\tau$. This is confirmed by the power density spectrum of the turbulent kinetic energy (TKE) also presented on Figure 4. A clear peak is identified at $St = f\tau \sim 0.6$ with a small harmonic at $St \sim 1.2$. This value is well in line with the data reported in the literature (Syred, 2006). Figure 5 shows a 3D visualization of the coherent motion using the λ_2 technique. The vortex core is aligned with the axis of symmetry in the upstream tube but undergoes a strong off-axis motion close to the expansion. This motion is referred to in the literature as precessing vortex core (PVC). Figure 5 also shows that the ordered vortex structure (spiral like) breaks down in the recirculation zone into smaller scale less ordered vortices.

Statistical quantities describing the PVC have been extracted using POD. Figure 5 shows the TKE content of the POD modes. A pair of modes clearly dominates the distribution with $\sim 10\%$ of the TKE each. It should be pointed out that the fraction of TKE presented in Figure 5 refers to the total TKE in the considered domain (i.e. the whole computational geometry). Although mode 1 contains 10% of the total TKE, it may represent ~ 20 or 30% of the TKE at a given location. We study the structure of the coherent structure isolated into mode 1 and 2. Figure 6 shows a visualization of the vortices corresponding to mode 1 and 2. Each mode consists of a pair of counter-rotating vortices. These vortices are shaped like a double helix that originates $\sim 1D$ upstream of the expansion. The double helix covers the region of vortex-breakdown. Note that mode 1 and 2 are anti-symmetric if rotated by an angle π around the axis. Further, we see that mode 2 is almost identical to mode 1 but is shifted by $\pi/2$ considering a rotation around the axis. Figure 7 shows the POD time coefficients $a_i(t)$ presented in the Fourier-space. Mode 1 and 2 are characterized by a single well defined peak at $St \sim 0.6$ which corresponds to the PVC characteristic frequency. Figure 7 also indicates that $a_1(t)$ and $a_2(t)$ have a phase shift of $-\pi/2$ so that mode 1 and 2 are orthogonal both in space and time. The combination of mode 1 and 2 results in a rotation of the double helix in time around the axis. It follows that the PVC can be represented by a helical wave as pointed out by Fernandes et al. (2006).

SUMMARY

Large Eddy Simulation of vortex breakdown in a swirling flow has been performed. The numerical results indicate that vortex breakdown induces the formation of two recirculation zones (CRZ and TRZ) downstream of the expansion. The results have been found weakly sensitive to the computational resolution and to the incoming velocity fluctuation. The LES captures well the flow both in terms of mean flow field and velocity fluctuations.

The unsteady flow features have been investigated. In particular, we identify an intense coherent motion. It

consists of an off-axis rotation of the vortex core at $St \sim 0.6$ and is referred to as PVC. The PVC has been isolated using POD applied on the 3D field. It has been shown that the PVC consists of a pair of counter-rotating helical vortices. This vertical structure rotates around the geometry axis with a frequency of $St \sim 0.6$. This may explain the reason why the PVC follows a helical wave as reported in the literature.

ACKNOWLEDGMENTS

This work has been supported by the Swedish Research Council (VR). The computations have been performed at LUNARC and HPC2N facilities within the SNAC/SNIC allocation program.

The authors want to thank Dr. Markus Klein (TU-Darmstadt, Germany) for kindly providing the code for generating the unsteady inflow conditions.

REFERENCES

- Berkooz G., Holmes P., Lumley J. L. 1993, "The Proper Orthogonal Decomposition in the Analysis of Turbulent Flows", *Annu. Rev. Fluid Mech.*, Vol. 25, pp. 539-575.
- Cala C.E., Fernandes E.C., Heitor M.V., Shtork S.I. 2006, "Coherent structures in unsteady swirling jet flow", *Exp. Fluids*, Vol. 40, pp. 267-276.
- Dellenback P.A., Metzger D.E., Neitzel G.P., 1988, "Measurements in turbulent swirling flow through an abrupt axisymmetric expansion", *AIAA J.*, Vol. 26, pp. 669-681.
- Fernandes E.C., Heitor M.V., Shtork S.I., 2006, "An analysis of unsteady highly turbulent swirling flow in a model combustor", *Exp. Fluids*, Vol. 40, pp. 177-187
- Fureby C., Grinstein F., 2002, "Large Eddy Simulation of High-Reynolds-Number Free and Wall-bounded flows", *J. Comp. Physics*, Vol. 181, pp. 68-77.
- Gullbrand J., Bai X.S., Fuchs L., 2001, "High-order Cartesian Grid Method for Calculation of Incompressible Turbulent Flows", *Int. J. Num. Meth. Fluids*, Vol. 36, pp. 687-709.
- Jeong J., Hussain F., 1995, "On the Identification of a Vortex", *J. Fluid Mech.*, Vol. 285, pp. 69-94.
- Klein M., Sadiki A., Janicka J., 2003, "A digital filter based generation of inflow data for spatially developing direct numerical or large eddy simulations", *J. Comp. Phys.* Vol. 186, pp. 652-665.
- Lucca-Negro O., O'Doherty T., 2001, "Vortex breakdown: a review", *Prog in Energy and Comb. Sci.*, Vol. 27, pp. 431-481.
- Sagaut P., 2001, "Large Eddy Simulation for Incompressible Flows", Springer Verlag.
- Schlüter J.U., Pitsch H., Moin P., 2004, "Large Eddy Simulation Inflow Conditions for Coupling with Reynolds-Averaged Flow Solvers", *AIAA J.*, Vol. 42, pp. 478-484.
- Smith T., Moehlis J., Holmes P., 2005, "Low-dimensional Modeling of Turbulence Using the Proper Orthogonal Decomposition: A Tutorial", *Nonlinear Dyn.*, Vol. 41, pp. 275-307.
- Syred N., 2006, "A review of oscillation mechanisms and the role of the precessing vortex core (PVC) in swirl combustion systems", *Prog in Energy and Comb. Sci.*, Vol. 32, pp. 93-161.

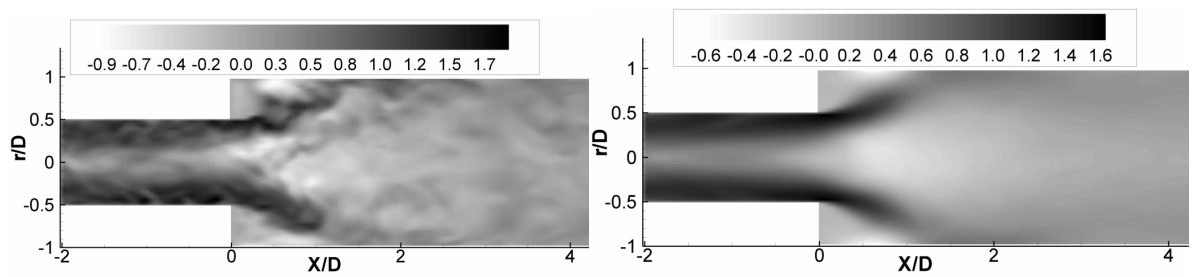


Figure 1: Instantaneous (left) and time averaged (right) normalized axial velocity field in a cut of the combustor (Case 3).

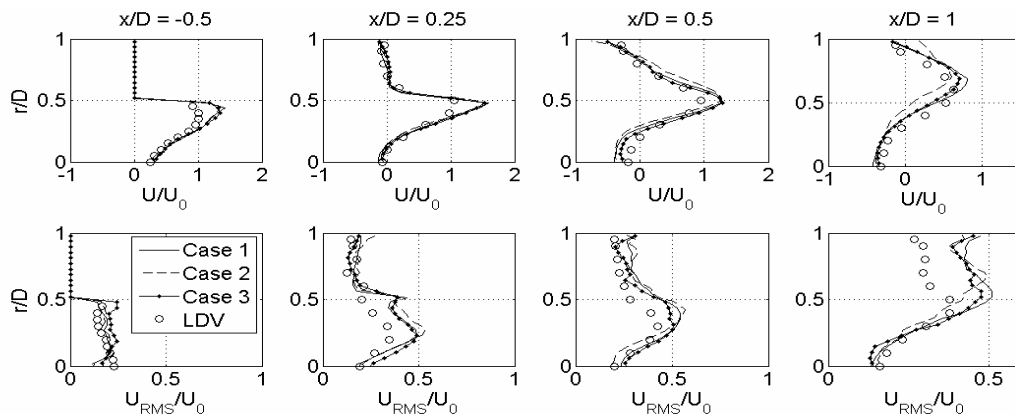


Figure 2: Normalized axial velocity along radial lines for cases 1, 2, 3 vs. LDV data: mean and RMS of the fluctuation.

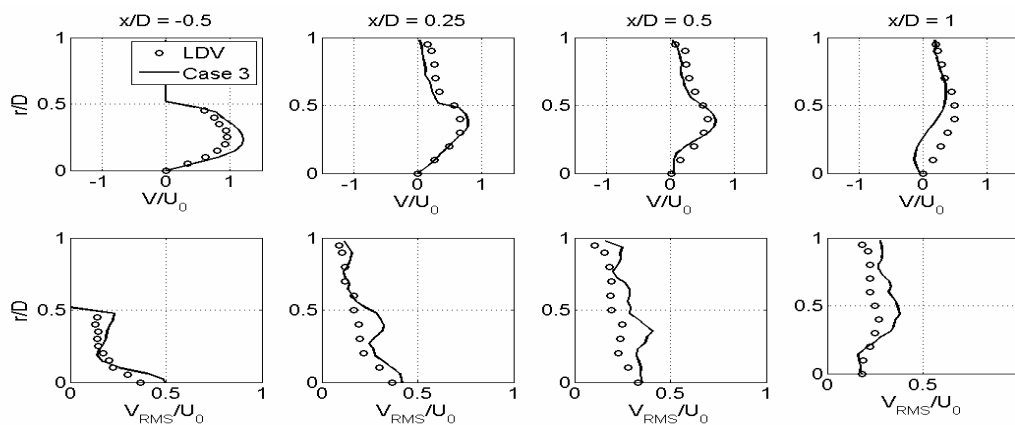


Figure 3: Normalized azimuthal velocity along radial lines for case vs. LDV data: mean and RMS of the fluctuation.

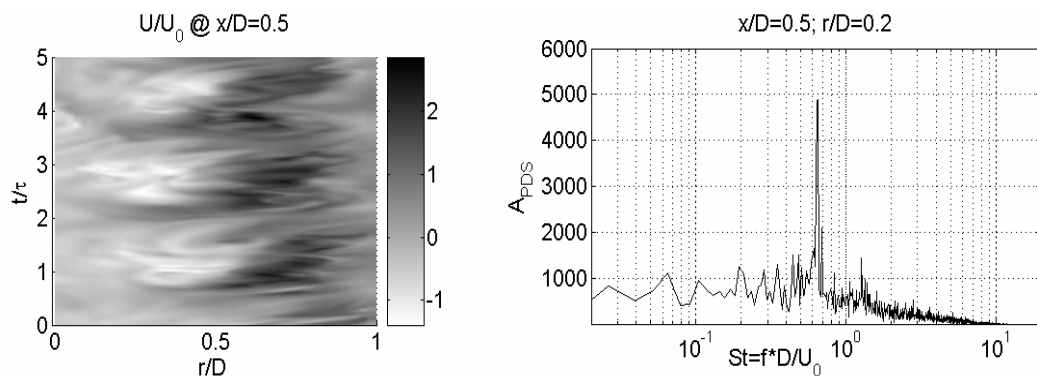


Figure 4: Left: normalized axial velocity along a radial line during $5 \cdot \tau$. Right: Power Spectra of the Turbulent Kinetic Energy at $[x/D=0.5; r/D=0.2]$.

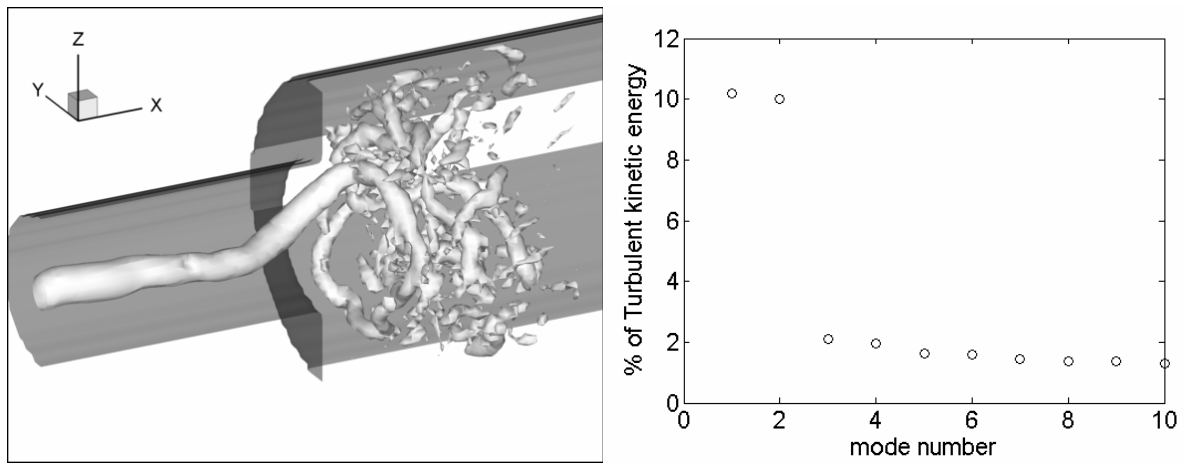


Figure 5: Left: snapshot of the instantaneous vortex core using the λ_2 technique. Right: distribution of the turbulent kinetic energy among the different POD modes.

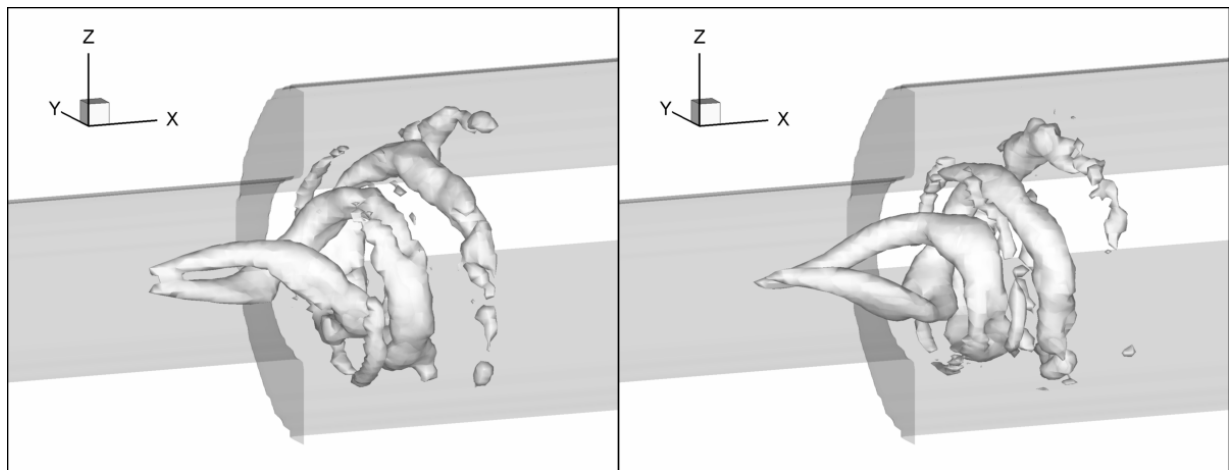


Figure 6: Visualization of the vortices core contained in mode 1 (left) and mode 2 (right) using the λ_2 technique.

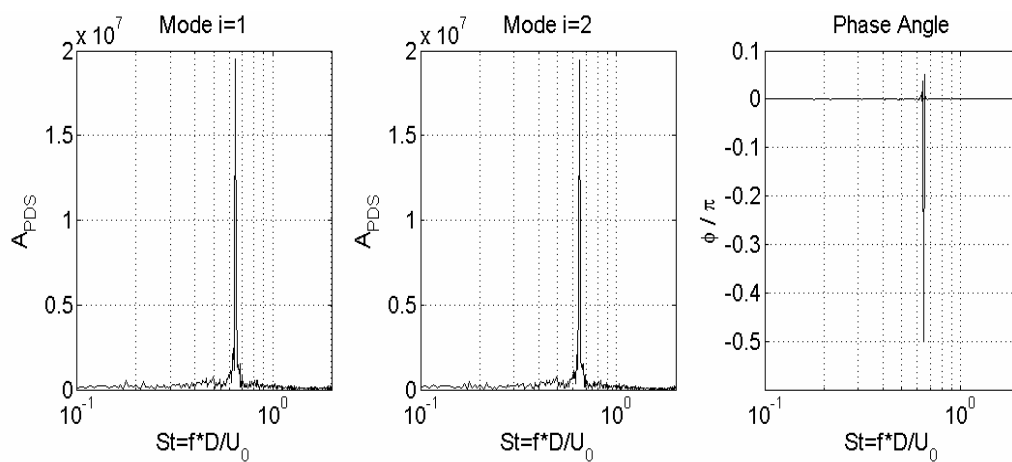


Figure 7: representation of the POD time coefficients $a_i(t)$ in the Fourier space. Left: power spectrum of $a_1(t)$. Center: power spectrum of $a_2(t)$. Right: phase difference between $a_1(t)$ and $a_2(t)$.